Efficient Acousto-Optical Light Modulation at the Mid-Infrared Spectral Range by Planar Semiconductor Structures Supporting Guided Modes

Ivan M. Sopko,[1] Daria O. Ignatyeva,[1,2,†] Grigory A. Knyazev,[1,2,*] and Vladimir I. Belotelov[1,2]

[1] *Faculty of Physics, Lomonosov Moscow State University, Leninskie Gory, 119991 Moscow, Russia*

[2] *Russian Quantum Center, Novaya str., Skolkovo, 143025 Moscow, Russia*

(Received 20 June 2019; revised manuscript received 19 September 2019; accepted 27 February 2020; published 31 March 2020)

Acousto-optical devices, such as modulators, filters, or deflectors, implement a simple and effective way of light modulation and signal-processing techniques. However, their operation wavelengths are restricted to the visible and near-infrared frequency regions due to a quadratic decrease of the efficiency of acousto-optical interactions with increasing wavelength. At the same time, almost all materials with a high value of the acousto-optic figure of merit are nontransparent at wavelengths longer than 5 μm, while the transparent materials possess a significantly lower acousto-optic figure of merit. Here, we propose and demonstrate by calculations how these limitations can be overcome using specially designed planar semiconductor structures that support electromagnetic modes strongly coupled to the incident light in the Otto configuration. Such an approach can be used for an efficient acousto-optical device operating in the mid-infrared range of 8–14 μm. An acoustic wave excited by a piezoelectric transducer in a semiconductor prism is utilized to modulate the coupling coefficient of the incident light to the guided mode of the semiconductor structure, which results in up to 100% modulation of the transmitted light at a spatial scale less than the ultrasound wavelength. It allows the utilization of acoustic waves with a short decay distance, and therefore, it provides a unique possibility to achieve an efficient acousto-optical modulation at frequencies about 1 GHz, which are unreachable for traditional acousto-optics.

DOI: 10.1103/PhysRevApplied.13.034076

I. INTRODUCTION

Here, we propose to utilize an acoustically controlled prism coupling of light in planar semiconductor structures supporting guided modes to enhance the acousto-optic interaction in the mid-infrared range, in particular, at 10.6 μm wavelength. The considered structure is suitable for the following reasons. The vast majority of acousto-optic devices are intended for visible and near-infrared frequency ranges [1,2]. However, operation at the mid-infrared range is very promising due to the atmosphere's transparency window at 8–14 μm wavelengths and the fact that the thermal radiation maximum is within that range at room temperature. Nowadays, there is an active development of mid-infrared tunable filters and image-processing devices. In particular, there is a request for microscale light modulators with operational frequencies over 1 GHz [3]. To adapt acousto-optic devices and techniques to the mid- and far-infrared ranges, one has to overcome several challenges, most notable of which is the lack of materials with a high acousto-optic figure of merit that are transparent at wavelengths longer than 5–8 μm. Since the efficiency of the acousto-optic interaction decreases, according to quadratic law, with wavelength growth, materials with an extremely high acousto-optic figure of merit are highly in demand. Some of the unconventional materials proposed for such applications include single-crystal tellurium [4,5], KRS-5 crystals [6], crystalline iodic acid, and lithium iodate [7]. Additionally, the problem of operation at gigahertz frequencies is also quite challenging. The acoustic wave absorption scales quadratically with frequency, which leads to losses exceeding 10 dB/cm at 1 GHz for many acousto-optical materials [8]. As a result, the effective length of the acousto-optical interaction is less than 100 μm, which is negligible for bulk acousto-optics.

The significant enhancement of the acousto-optical interaction efficiency in the mid-IR region could be realized through excitation of optical modes, which are more sensitive than the bulk wave beams, in a multilayer medium. Similar structures are successfully used for the enhancement of the light-matter interaction in layered structures [9,10], where surface plasmon polaritons [11], localized surface plasmons [12], waveguide modes [13], and Tamm plasmons are excited [14]. Acoustic modulation of the prism coupling coefficient with plasmonic structures was used to detect an acoustic wave by visible light in Refs. [15,16].

*g_knyazev@mail.ru
†ignatyeva@physics.msu.ru

 © 2020 American Physical Society

Plasmonics in the mid-infrared range differ from conventional plasmonics of the visible range in terms of material properties and required techniques. The wave number of the surface plasmon for most metals is very close to the wave number of light, so that surface plasmons poorly penetrate into the metal layer, while the penetration depth in a dielectric significantly increases [17]. As a result, differences between the light incidence angle of the plasmon excitation and the angle of total internal reflection are negligible. This defines an extremely narrow resonance shape [12], which is challenging for implementation in real devices, but grants possibilities for a high modulation depth [18]. Another approach is to utilize phonon polaritons in a highly absorbent medium, such as silicon carbide [19]. In that case, the phonon resonance is similar to the plasmon one in the visible range.

Here, we consider two types of the structures: the positive permittivity semiconductor (PPS) structure, consisting of a GaAs prism and a thin film with an air gap in between, and the negative permittivity semiconductor (NPS) structure, where a SiC film is utilized. The SiC film has negative permittivity near 10 μm due to the phonon resonance, and therefore, it is supporting a surface phonon polariton mode. Modulation of the thickness of the gap between the prism and the semiconductor film that sustains optical mode results in a significant modulation of the coupling efficiency between the incident light and the guided mode, as well as in modulation of the mode propagation constant. It provides efficient modulation of the reflected light. Thus, we use the Otto configuration for excitation of the guided modes. The advantage of the Otto configuration is in the fact that the prism refractive index can be modulated via an acoustic wave propagating in the prism and reflecting from the gap boundary. As a result, there is no modulation of the guiding-layer parameters. At the same time, because of a high difference in acoustic impedances, the refractive index modulation achieved by means of acoustic waves excited with a piezoelectric transducer is estimated to be about up to 10^{-3}. We show that this level of modulation is enough to provide a large variation of the reflected light intensity up to 100% in the structures with high-quality-factor optical resonances.

II. ACOUSTO-OPTICAL MODULATION BASED ON COUPLING CONTROL

The principal scheme of the proposed modulator is shown in Fig. 1(a). The incident light impinges on the prism and, due to the attenuated total internal reflection, excites a waveguide mode in the PPS structure or a surface phonon polariton in the NPS structure. We use the Otto geometry of prism coupling, since it allows for coupling control via acoustic waves, as discussed in the Sec. III. A prism made from an infrared-transparent material with a high refractive index, such as GaAs or Ge, is located above the multilayered structure with an air gap of about 1 μm. The longitudinal acoustic wave with power density W, excited via a piezoelectric transducer placed on top of the prism, provides variations of both the air gap thickness, δd, and prism dielectric permittivity, $\delta\varepsilon_p$. We show in Part I of the Supplemental Material [20] that δd depends on the frequency of ultrasound. As a result, at low frequency, it is necessary to take into account both δd and $\delta\varepsilon_p$. Analysis shows that, in the case of positive photoelastic constants of $Bi_{12}GeO_{20}$, CdS, and KRS-5, the influence of $\delta\varepsilon_p$ and δd on the reflection coefficient is cumulative and subtractive for materials with a negative photoelastic constant, such as GaP, Ge, and GaAs. However, at frequencies above 100 GHz, only perturbation of the dielectric constant plays a significant role in light modulation. Therefore, in analytical theory, we take into account both δd and $\delta\varepsilon_p$, but in numerical calculations performed at a frequency of 1 GHz modulation of the thickness of the air gap, δd, plays an insignificant role.

The magnitudes of the air gap and dielectric permittivity modulation for different infrared materials and 1 GHz frequency of the acoustic wave are shown in Fig. 1(b). We choose to use a GaAs prism for our research due to its relatively large absolute value of $\delta\varepsilon_p$, which is especially important at high frequencies.

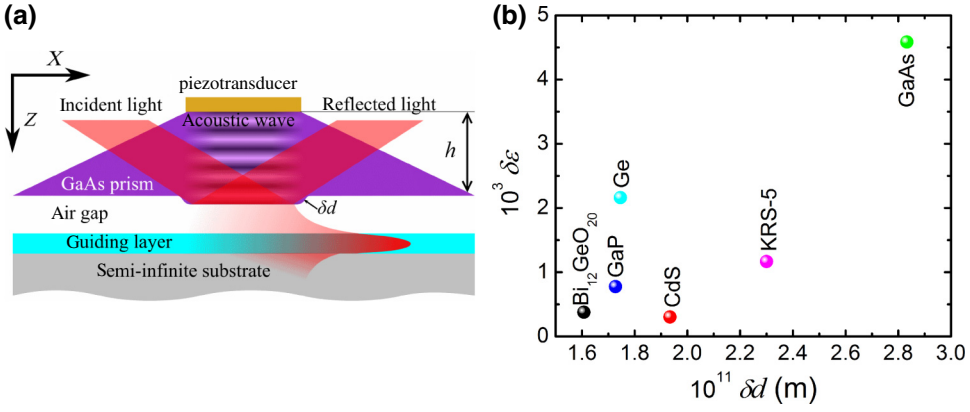

FIG. 1. Acousto-optical light modulation via excitation of optical modes in the Otto configuration: (a) modulator principal scheme; (b) comparison of different infrared materials for the prism. Acoustic power density is assumed to be $W = 1\,\mathrm{W/mm^2}$; frequency of ultrasound is $f = 1$ GHz.

To analyze the influence of the prism dielectric permittivity and gap-thickness variation on the coupling efficiency in the Otto configuration, it is necessary to solve wave equations with boundary conditions for E_y and H_x for s-polarized light and for E_x and H_y for p-polarized light, in the case of attenuated total internal reflection at the prism-air interface. The method for calculation of reflection from the layered waveguide or surface-wave-supporting structures is mathematically similar to the one used to describe multilayered antireflection optical coating [21] and is generalized for the case of the imaginary k_z wave vector component arising in some layers of the analyzed structures.

III. ACOUSTO-OPTICAL MODULATION IN THE STRUCTURE WITH A NEGATIVE PERMITTIVITY SEMICONDUCTOR

It is advantageous to use silicon carbide for the NPS structure. It is a semiconductor material that has a resonant absorbance peak at 10.6 μm with a dielectric permittivity of $\varepsilon_{\mathrm{SiC}} = -1.46 + 0.15i$. This allows for excitation of the surface phonon polaritons at the SiC-air interface. Similarly to surface plasmon polaritons, excitation of the surface phonon polaritons is possible only in the case of p-polarized light. Phonons in the IR range resemble plasmons in the visible range: they have a relatively wide resonance and propagation length comparable to that of the wavelength of radiation. We start our study by analyzing surface phonon excitation on the silicon carbide/air interface with the prism method in the Otto configuration.

Implementing the methodology introduced in Refs. [14,16,19,22] for the case of the Otto configuration, we get reflection coefficient R in the case of a wide gap, $\exp(-2k_{1z}d) \ll 1$:

$$R(k_x) = \left|\frac{k_{0z}/\varepsilon_p - k_{1z}/\varepsilon_{\mathrm{air}}}{k_{0z}/\varepsilon_p + k_{1z}/\varepsilon_{\mathrm{air}}}\right|^2 \times \left(1 - \frac{4\beta''\,\Delta\beta''}{[k_x - (\beta' + \Delta\beta')]^2 + (\beta'' + \Delta\beta'')^2}\right), \tag{1}$$

where k_{0z} and k_{1z} are wave vector components orthogonal to layers of the structure in the prism and in the air gap, respectively; $\beta = \beta' + i\beta''$ is a wave number of the surface mode at the guiding layer/air interface without consideration of the prism's influence. Prism coupling results in the wave number shift $\Delta\beta$. The real part of this shift, $\Delta\beta'$, corresponds to a change in resonance position, while the imaginary part, $\Delta\beta''$, leads to symmetrical variations of the resonance width and depth.

Obtaining expressions for the dispersion of surface phonon polaritons on a thin film in an asymmetric environment, similarly to Ref. [21], one finds that the wavevector of the normal mode of the structure acquires an additional term caused by prism coupling:

$$\Delta\beta = \left(\frac{\omega}{c}\right)\frac{k_{0z}/\varepsilon_p - k_{1z}/\varepsilon_{\mathrm{air}}}{k_{0z}/\varepsilon_p + k_{1z}/\varepsilon_{\mathrm{air}}}\exp(-i2k_{1z}d)C(\varepsilon_j,\ d_j), \tag{2}$$

where C is a parameter that depends on the thicknesses and dielectric permittivities of the layers, not including the prism. The value of $C(\varepsilon_j,\ d_j)$ for the three-layer structure GaAs-air-SiC can be calculated with the approximation $\varepsilon''_{\mathrm{SiC}} \ll |\varepsilon'_{\mathrm{SiC}}|$:

$$C = \frac{2}{\varepsilon_{\mathrm{SiC}} - \varepsilon_{\mathrm{air}}}\left(\frac{\varepsilon_{\mathrm{SiC}}\varepsilon_{\mathrm{air}}}{\varepsilon_{\mathrm{SiC}}^2 + \varepsilon_{\mathrm{air}}^2}\right)^{3/2}. \tag{3}$$

It should be noted that the influence of air-gap-thickness variation, δd, and changes in dielectric permittivity of the prism, $\delta\varepsilon_p$, do not depend on the structure's properties. Additionally, due to total internal reflection, k_{1z} is imaginary, so the exponent of power in Eq. (2) is real. Thus, the acoustic wave affects both resonance shape and position; however, reflectance is modulated mostly by the resonance position shift.

Notably, the addition to the phonon polariton wave number is equivalent to the variation of the light incidence angle at which the resonance is observed: $\Delta\beta = \Delta\theta\cos\theta\sqrt{\varepsilon_p}\omega/c$. Because the acoustic interaction occurs through prism coupling by means of variations in δd and $\delta\varepsilon_p$, the resonance shift $\delta\theta$ caused by the acoustic wave can be acquired from Eq. (2):

$$\delta\theta|_{\varepsilon=\mathrm{const}} = -2\delta d\frac{|k_{1z}|}{k_{0z}}(\Delta\beta' + i\Delta\beta''), \tag{4}$$

$$\delta\theta|_{d=\mathrm{const}} = \delta\varepsilon_p\frac{|k_{1z}|(\varepsilon_{\mathrm{air}} + \varepsilon_p)}{k_{0z}^2\varepsilon_{\mathrm{air}}^2 - k_{1z}^2\varepsilon_p^2}(\Delta\beta'' - i\Delta\beta'). \tag{5}$$

Notably, the value of radiation losses can also be controlled by the air-gap thickness. As follows from Eq. (1), the optimal value of d is determined by the condition $\Delta\beta'' = -\beta''$. Because the angular shift $\delta\theta$ caused by $\delta\varepsilon_p$ variation depends on $\Delta\beta''$ linearly, the contribution of $\delta\varepsilon_p$ to the modulation of reflectance is weakly dependent on the resonance width, while the contribution of δd is strongly affected by the resonance width. Further analysis shows that, at the given value of the acoustic power density, the variation of the prism's dielectric permittivity, $\delta\varepsilon_p$, corresponds to the shift angle $\delta\theta = 0.1°$ for the examined structures. This means that at low ultrasound frequency, where both δd and $\delta\varepsilon_p$ are significant for resonances narrower than 1°, the contribution of $\delta\varepsilon_p$ prevails over the influence of δd, while for wider resonances δd is most important. However, as follows from Eqs. (S1.4)

and (S1.6) within the Supplemental Material [20], with an increase in the acoustic frequency, the contribution of δd decreases, and the influence of $\delta\varepsilon_p$ is independent of frequency. Therefore, at frequencies of about 1 GHz, the contribution of δd becomes insignificant and modulation is defined by $\delta\varepsilon_p$ for any resonance width.

To calculate the modulation efficiency, ζ, caused by acoustic waves, we calculate reflection indices for two full shift positions: $R = R(d-\delta d,\ \varepsilon_p - \delta\varepsilon_p)$ and $R_+ = R(d+\delta d,\ \varepsilon_p + \delta\varepsilon_p)$. The modulation efficiency of the reflected beam ζ is defined by

$$\zeta = \frac{\delta R}{2\langle R\rangle} = \frac{R_- - R_+}{R_- + R_+}. \tag{6}$$

In the basic case of the GaAs prism/air gap/semi-infinite SiC layer, the deepest resonance of $R_{\min} = 18\%$ reflectance is achieved for an air-gap thickness of 970 nm at an incidence angle value of 45.1°. In Fig. 2(a), the reflectance and modulation coefficient ζ for the dielectric permittivity modulation of $\delta\varepsilon_p = 0.0046$ are represented; in the inset, a temporal dependence of reflectance in the case of harmonic acoustic oscillation is shown. It is seen that modulation is close to a sinusoidal shape. This trend is explained by the relatively low level of modulation coefficient, $\zeta < 0.6\%$.

The practical advantage of this structure is a wide band of possible light incidence angles, $\Delta\theta = 15°$. This configuration due to a wide resonance shape possesses a very high tolerance to operating wavelength variation, $\partial R_{\min}/\partial\lambda = 10^{-4}\%/\text{nm}$. The structure may be easily miniaturized to increase the operation frequency limit caused by dissipation of the acoustic beam.

Figure 2(b) demonstrates a spatial distribution of the electromagnetic field. The distribution of the field proves that, on the surface of SiC, a surface phonon polariton is excited. As shown by the blue curve in Fig. 2(b), modulation of the electric field achieves the highest values on the surface of SiC, but not in the prism. This means that the double-layer NPS structure is not optimal for the modulation of light. The curve is plotted for the incidence angle corresponding to the highest modulation of R [see Fig. 2(a)].

To achieve deeper and narrower resonances, it is possible to utilize thin SiC films on the substrate (for example, ZnS with $n = 2.21$) that allow for simultaneous control of the coupling coefficient and internal damping. The best results are achieved for the NPS structure containing a 570-nm thick SiC layer with a 433 nm air gap. The resulting resonance reaches $R_{\min} = 0.05\%$ at 52.7° [see Fig. 3(a)]. This minimum reflectance value is chosen to mimic the small background always present due to the roughness of the layer surfaces and width inaccuracies, to avoid artificial overstatement of modulation efficiency due to the near-zero denominator in Eq. (8). The angle of total internal reflection for the GaAs/ZnS interface is 42.52°, which results in a singular spike on the graph. Excitation of the optical mode in examined in our structures allows one to obtain quadratic or linear acousto-optical modulation, depending on the angle of incidence. To obtain quadratic modulation, it is necessary that the optical incidence angle corresponds to the minimum of the reflection curve, while a linear regime is observed at some mismatch from the center of resonance. In the inset of Fig. 3(a), linear (black curve) and quadratic (blue curve) regimes of R modulation are shown. This structure provides almost 20% linear modulation. The described scheme is also tolerant to variation of the operating wavelength to less than $2\times10^{-4}\%/\text{nm}$. Because this structure possesses three layers, it is possible to calculate the sensitivity to variation of the SiC layer thickness, $\partial R_{\min}/\partial d_{\text{SiC}} = 0.01\%/\text{nm}$. Thus, this structure is quite tolerant to changes in its parameters.

The distribution of the electromagnetic field in Fig. 3(b) demonstrates excitation of a surface mode in the guiding layer of SiC. An exponential decrease of the magnetic field

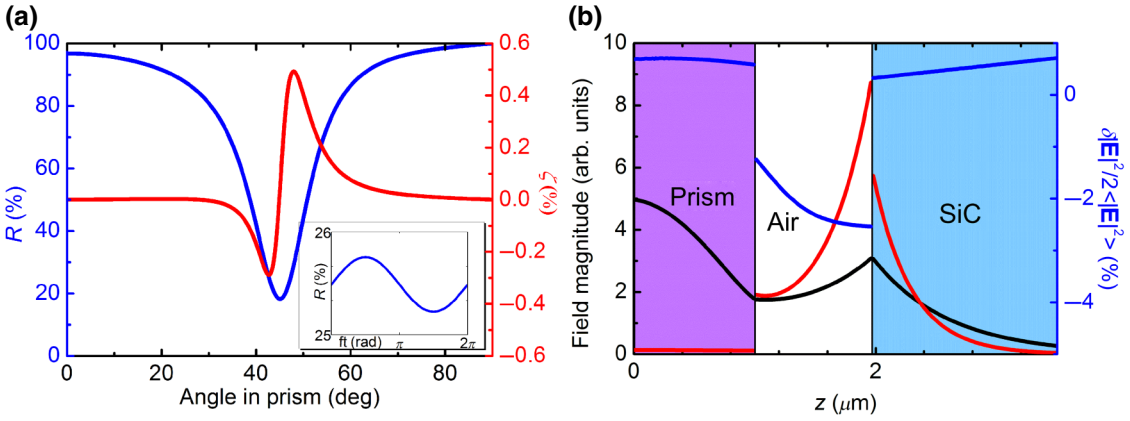

FIG. 2. Acousto-optical modulation enhanced via excitation of phonon polaritons in SiC. (a) Angular spectra of reflectance R and modulation coefficient ζ and temporal dependence of R (inset). (b) Spatial distribution of electromagnetic field H_y (black) and $|\mathbf{E}|^2$ (red) and its modulation $\delta|\mathbf{E}|^2/2 < |\mathbf{E}|^2 >$ (blue) due to acoustic oscillations inside the structure.

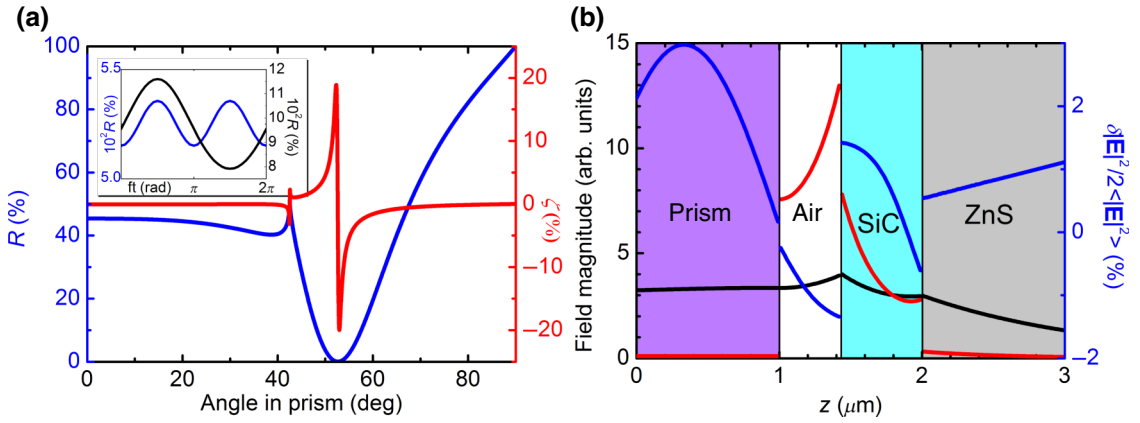

FIG. 3. Acousto-optical modulation enhanced via excitation of phonon polaritons in the SiC layer with ZnS substrate. (a) Angular spectra of reflectance R and modulation coefficient ζ and temporal dependence of R (inset). (b) Spatial distribution of electromagnetic field H_y (black) and $|\mathbf{E}|^2$ (red) and its modulation $\delta|\mathbf{E}|^2/2 < |\mathbf{E}|^2 >$ (blue) due to acoustic oscillations inside the structure.

in the air gap and the substrate may be observed. The higher value of electric field modulation [compare with Fig. 2(b)] in the prism, with respect to modulation of the field in the SiC layer, proves the validity of the application of the NPS structures.

IV. ACOUSTO-OPTICAL MODULATION IN POSITIVE PERMITTIVITY SEMICONDUCTOR STRUCTURES

To achieve high sensitivity for photoelastic variation of permittivity, we propose using PPS waveguide structures due to lower attenuation and a higher Q factor. Similar to the structures with SiC analyzed, a longitudinal acoustic wave is used to modulate the dielectric permittivity of the prism. However, opposite to the surface phonon polaritons, the excitation of TM or TE waveguide modes allows the utilization of both s- and p-polarized light. Implementation of waveguides with a high contrast of refraction index, such as air-GaAs-LiF allows deep resonances to be achieved with a minimal value of R up to 0.05% reflection.

Optimizing parameters of the structures for TM mode, we obtain an angular width of the resonance of 0.5° in the prism. In the case of p-polarized light, the optimal waveguide configuration is a 1.59 μm air gap, 1.8 μm GaAs core ($n = 3.27$), and LiF substrate ($n = 1.055$) with a resonance angle of 36.23°. Tolerance of the operating wavelength variation is about 0.002%/nm and sensitivity to variation of the GaAs waveguide layer thickness is slightly less than 0.01%/nm. In Fig. 4(a), angular distributions of the reflectance and modulation ζ are shown, while Fig. 4(b) shows the field distribution inside the structure and its variation. It is seen that application of the PPS structure provides the highest possible value of modulation, $\zeta = 100\%$. Modulation of the reflectance is nonlinear

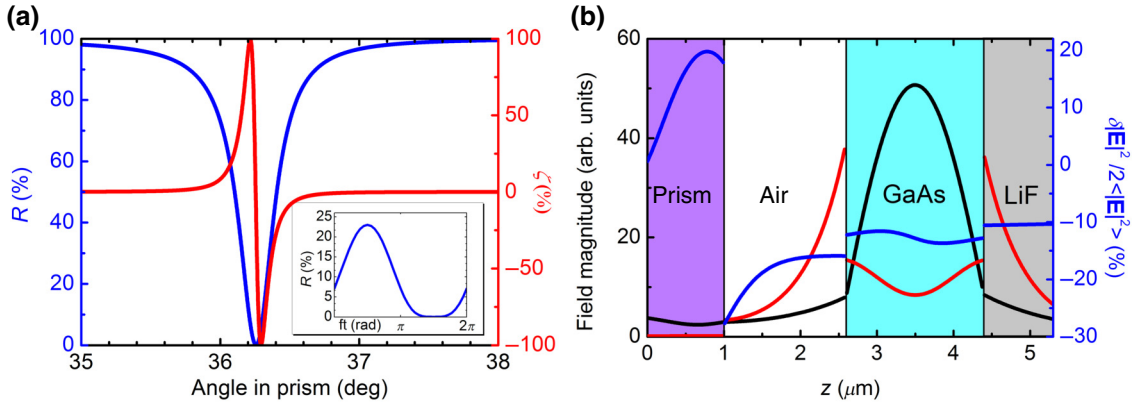

FIG. 4. (a) Acousto-optical modulation enhanced via excitation of waveguide mode in the air-GaAs-LiF waveguide in p-polarized light. (a) Angular spectra of reflectance R and modulation coefficient ζ and temporal dependence of R (inset). (b) Spatial distribution of electromagnetic field H_y (black) and $|\mathbf{E}|^2$ (red) and its modulation $\delta|\mathbf{E}|^2/2 < |\mathbf{E}|^2 >$ (blue) due to acoustic oscillations inside the structure.

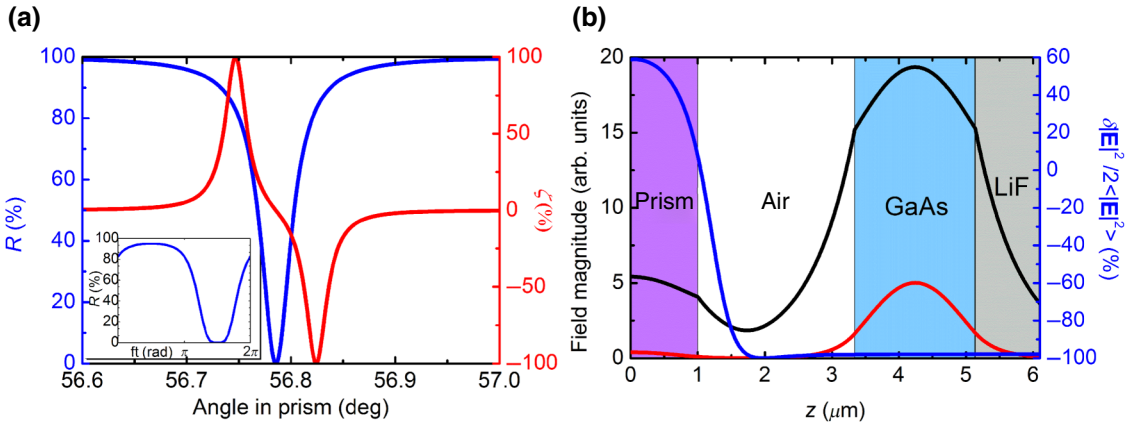

FIG. 5. Acousto-optical modulation enhanced via excitation of waveguide mode in the air-GaAs-LiF waveguide in *s*-polarized light. (a) Angular spectra of reflectance R and modulation coefficient ζ. (b) Spatial distribution of electromagnetic field H_y (black) and $|\mathbf{E}|^2$ (red) and its modulation $\delta|\mathbf{E}|^2/2 < |\mathbf{E}|^2 >$ (blue) due to acoustic oscillations inside the structure.

[inset of Fig. 4(a)]. The modulated signal acquires a square shape, rather than a sinusoidal one, with a further increase in the acoustic power density W.

We obtain a narrower resonance in the structure optimized for TE mode. Due to the higher Fresnel coefficients, *s*-polarized light provides narrower resonances of $\Delta\theta = 0.1°$, which are actually narrower than the value of the shift, due to the acoustic wave. To achieve 0.05% reflectance minimum at 56.78°, we use the PPS structure with a 2.33 μm air gap and 1.8 μm GaAs core. Sensitivity to both variations of GaAs waveguide layer thickness and operating wavelength is about 0.002%/nm. The characteristics of this structure are shown in Fig. 5. The modulation of light is nonlinear [see the inset in Fig. 5(a)] and its time dependence also has a square shape, the duty cycle of which is controlled by the acoustic power density. To obtain a linear regime, it is necessary to decrease the power density by about six times.

In Fig. 5(b), huge modulation of the electric field is demonstrated. If we use an optical fiber to output optical radiation from the guiding layer, it will provide higher values of modulation. In this case, the modulation efficiency of light will increase with the width of the acoustic impact region. However, an important advantage of the device proposed here will be lost, namely, the possibility of modulation at frequencies above 1 GHz. With increasing width of the acoustic beam, the electric capacitance of the piezoelectric transducer increases. As a result, the excitation of acoustic waves at high frequencies will be extremely difficult and the modulation depth will be low.

Waveguides with lower dielectric contrast, such as air-GaAs-CdTe or air-ZnS-LiF, are also analyzed. Although optimal matching conditions for excitation of the waveguide resonance with $R_{\min} = 0.05\%$ can also be realized, acousto-optical modulation of the signal will be several times weaker. This is caused by less-efficient energy localization in the waveguide core, which makes the structure less sensitive to coupling modulation.

V. DISCUSSION

To achieve a high modulation frequency in the studied structures, it is necessary to overcome several limitations. We consider the mechanisms in detail in Part II of the Supplemental Material [20]. The calculated frequency limits for each of the structures are presented in Table I.

Limitations are caused by the fact that the piezoelectric transducer is located at some distance, h (see Fig. 1),

TABLE I. Ultrasound frequency limits for the studied structures due to various factors.

Structure	Angle of incidence (deg)	Angular width of incident light (deg)	Length of acoustic beam h (mm)	Frequency limits (GHz)			
				Acoustic attenuation	Uniform modulation of ε_p	Intersection of diffraction orders	Diffraction limit
GaAs-air-SiC	45.06	6.60	0.01	10.96	0.23	0.41	2.08
GaAs-air-SiC-ZnS	52.70	3.00	0.02	7.84	0.12	0.23	2.35
GaAs-air-GaAs-LiF, *p*-pol.	36.23	0.09	1.10	1.17	0.003	0.005	1.74
GaAs-air-GaAs-LiF, *s*-pol	56.78	0.02	3.50	0.65	0.001	0.002	2.46

from the GaAs-air interface. This distance is defined by the width of the incident-light angular spectrum, correlating to modulation value ζ attenuation at -3 dB level (see column 3 of Table I). The fifth column of Table I represents the limitation caused by ultrasound attenuation [23] at distance h. Although it allows modulation at rather high frequencies, it is impossible to excite an acoustic wave above that limit. The sixth column shows a strict frequency limit for the case of homogenous disturbance of the prism's dielectric permittivity. Above these frequency values, the disturbance of dielectric permittivity will be inhomogeneous. This will lead to the appearance of several light diffraction orders [24]. However, while the first diffraction order overlaps with the zero-diffraction order, the modulation intensity will be similar to that of the homogenous case. Diffraction order overlap is observed at frequencies up to the limit presented in the seventh column of Table I. Above these frequencies, modulation can be achieved only in the case of the oblique incidence of ultrasound at the prism-air interface. Modulation of the light intensity will be observed only in -1 and $+1$ diffraction orders. Variation of light intensity will be similar to the low-frequency case. This feature will be observed only while the diffraction of light at an inhomogeneous disturbance of dielectric permittivity ε is possible.

At frequencies presented in the eighth column of Table I, the diffraction disappears as the period of inhomogeneity becomes too small. Nevertheless, it is possible to observe quadratic modulation [see inset in Fig. 2(a)], and the modulation frequency will turn out to be twice the frequency of the ultrasound. Unfortunately, quadratic modulation does not allow us to overcome the limit caused by ultrasound attenuation, so it is appropriate for SiC-based structures. For the case of the semi-infinite SiC layer, quadratic modulation turns out to be extremely weak: 0.003%. However, for the GaAs-air-SiC-ZnS structure, quadratic modulation is around 4%.

An alternative method to avoid restrictions on the modulation frequency is to excite ultrasound from the substrate side [see Fig. 1(a)]. However, in this case, the acoustic problem becomes much more complicated. For example, you must consider the possibility of forming a surface acoustic wave in the guiding layer. Moreover, it is necessary to select the guiding-layer material not only with acceptable optical properties, but also with appropriate acousto-optical properties. Nevertheless, for the case of excitation of ultrasound from the substrate, the results and analytical methods presented here remain valid.

VI. CONCLUSION

Application of the NPS structures allows modulation of a beam with a wide angular spectrum to be achieved, while the PPS waveguides provide a higher modulation coefficient, ζ. In terms of efficiency, most potential for acousto-optical modulation in the mid-IR region is found for the PPS waveguide structures. Excitation of TM or TE guided modes produces narrow and deep resonances, which make it possible to achieve extremely high modulation values, ζ. However, from the point of view of high-frequency modulation, NPS structures are more promising. Because of wide-angle absorption resonances, these structures provide modulation at frequencies of several gigahertz.

ACKNOWLEDGMENTS

This work is financially supported by the Russian Foundation for Basic Research (RFBR, Grant No. 18-29-20113).

[1] N. Savage, Acousto-optic devices, Nat. Photonics **4**, 728 (2010).

[2] C. S. Tsai, ed., *Guided-Wave Acousto-Optics: Interactions, Devices, and Applications*, Springer Series in Electronics and Photonics (Springer-Verlag, Berlin Heidelberg, 1990).

[3] B. Zeng, Z. Huang, A. Singh, Y. Yao, A. K. Azad, A. D. Mohite, A. J. Taylor, D. R. Smith, and H.-T. Chen, Hybrid graphene metasurfaces for high-speed mid-infrared light modulation and single-pixel imaging, Light: Sci. Appl. **7**, 51 (2018).

[4] L. E. Kreilkamp, I. A. Akimov, V. I. Belotelov, B. A. Glavin, L. V. Litvin, A. Rudzinski, M. Kahl, R. Jede, M. Wiater, T. Wojtowicz, G. Karczewski, D. R. Yakovlev, and M. Bayer, Terahertz dynamics of lattice vibrations in Au/CdTe plasmonic crystals: Photoinduced segregation of Te and enhancement of optical response, Phys. Rev. B **93**, 125404 (2016).

[5] N. Gupta, V. B. Voloshinov, G. A. Knyazev, and L. A. Kulakova, Optical transmission of single crystal tellurium for application in acousto-optic cells, J. Opt. **13**, 055702 (2011).

[6] V. B. Voloshinov, D. L. Porokhovnichenko, and E. A. Dyakonov, Optimization of acousto-optic interaction geometry in KRS-5 crystal for far-infrared applications, Opt. Eng. **56**, 087102 (2017).

[7] D. L. Porokhovnichenko, V. B. Voloshinov, E. A. Dyakonov, G. A. Komandin, I. E. Spektor, and V. D. Travkin, Application potential of paratellurite and iodic acid crystals for acousto-optics in the Terahertz range, Phys. Wave Phen. **25**, 114 (2017).

[8] J. E. B. Oliveira and C.-K. Jen, Backward collinear acoustooptic interactions in bulk materials, Appl. Opt. **29**, 836 (1990).

[9] G. A. Knyazev, P. O. Kapralov, N. A. Gusev, A. N. Kalish, P. M. Vetoshko, S. A. Dagesyan, A. N. Shaposhnikov, A. R. Prokopov, V. N. Berzhansky, A. K. Zvezdin, and V. I. Belotelov, Magnetoplasmonic crystals for highly sensitive magnetometry, ACS Photonics **5**, 4951 (2018).

[10] D. O. Ignatyeva, P. O. Kapralov, G. A. Knyazev, S. K. Sekatskii, G. Dietler, M. Nur-E-Alam, M. Vasiliev, K.

Alameh, and V. I. Belotelov, High-Q surface modes in photonic crystal/iron garnet film heterostructures for sensor applications, JETP Lett. **104**, 679 (2016).

[11] A. N. Kalish, R. S. Komarov, M. A. Kozhaev, V. G. Achanta, S. A. Dagesyan, A. N. Shaposhnikov, A. R. Prokopov, V. N. Berzhansky, A. K. Zvezdin, and V. I. Belotelov, Magnetoplasmonic quasicrystals: An approach for multiband magneto-optical response, Optica **5**, 617 (2018).

[12] D. Gérard, V. Laude, B. Sadani, A. Khelif, D. Van Labeke, and B. Guizal, Modulation of the extraordinary optical transmission by surface acoustic waves, Phys. Rev. B **76**, 235427 (2007).

[13] A. N. Kalish, D. O. Ignatyeva, V. I. Belotelov, L. E. Kreilkamp, I. A. Akimov, A. V. Gopal, M. Bayer, and A. P. Sukhorukov, Transformation of mode polarization in gyrotropic plasmonic waveguides, Laser Phys. **24**, 094006 (2014).

[14] V. N. Konopsky, Plasmon-polariton waves in nanofilms on one-dimensional photonic crystal surfaces, New J. Phys. **12**, 093006 (2010).

[15] R. Nuster, G. Paltauf, and P. Burgholzer, Comparison of surface plasmon resonance devices for acoustic wave detection in liquid, Opt. Express **15**, 6087 (2007).

[16] A. A. Kolomenskii, E. Surovic, and H. A. Schuessler, Optical detection of acoustic waves with surface plasmons, Appl. Opt. **57**, 5604 (2018).

[17] Y. Fuzi, G. W. Bradberry, and J. R. Sambles, Infrared surface plasmon-polaritons on Ni, Pd and Pt, J. Mod. Opt. **36**, 1405 (1989).

[18] I. M. Sopko and G. A. Knyazev, Plasmonic enhancement of mid- and far-infrared acousto-optic interaction [Invited], Appl. Opt. **57**, C42 (2018).

[19] H. C. Kim and X. Cheng, Surface phonon polaritons on SiC substrate for surface-enhanced infrared absorption spectroscopy, J. Opt. Soc. Am. B **27**, 2393 (2010).

[20] See the Supplemental Material at http://link.aps.org/supplemental/10.1103/PhysRevApplied.13.034076 for dielectric permittivity modulation depth and mechanisms of restriction analysis.

[21] H. Raether, *Surface Plasmons on Smooth and Rough Surfaces and on Gratings*, Springer Tracts in Modern Physics (Springer-Verlag, Berlin Heidelberg, 1988).

[22] E. Kretschmann, Die Bestimmung optischer Konstanten von Metallen durch Anregung von Oberflächenplasmaschwingungen, Z. Physik **241**, 313 (1971).

[23] J. Sapriel, P. Renosi, and P. Le Berre, in *SPIE Proceedings Acousto-Optics and Applications II*, edited by A. Sliwinski, P. Kwiek, B. B. J. Linde, A. Markiewicz, eds. (International Society for Optics and Photonics, Gdansk-Jurata, Poland, 1995), Vol. 2643, pp. 257.

[24] D. Royer and E. Dieulesaint, *Elastic Waves in Solids II: Generation, Acousto-Optic Interaction, Applications*, Advanced Texts in Physics, Elastic Waves in Solids (Springer-Verlag, Berlin Heidelberg, 2000).